AD-A070 491 CALIFORNIA UNIV LOS ANGELES PLASMA PHYSICS GROUP F/G 20/9
SIMULATION OF LOWER-HYBRID HEATING IN A NONUNIFORM PLASMA SLAB.--ETC(U)
MAY 79 V K DECY, G M MORALES, J M DAWSON N00014-75-C-0476

UNCLASSIFIED PPG-411 NL

1 OF 1
AD
A070491

END
DATE
FILMED
7-79
DDC

UCLA

LEVEL II

DDC
RECEIVED
JUN 27 1979
C

CENTER FOR
PLASMA PHYSICS
AND
FUSION ENGINEERING

UNIVERSITY OF CALIFORNIA
LOS ANGELES

06 26 070

SECURITY CLASSIFICATION OF THIS PAGE (When Data Entered)

REPORT DOCUMENTATION PAGE

READ INSTRUCTIONS BEFORE COMPLETING FORM

1. REPORT NUMBER (6)
2. GOVT ACCESSION NO.
3. RECIPIENT'S CATALOG NUMBER (9)

4. TITLE (and Subtitle)
SIMULATION OF LOWER-HYBRID HEATING IN A NONUNIFORM PLASMA SLAB

5. TYPE OF REPORT & PERIOD COVERED
Technical Rept.

6. PERFORMING ORG. REPORT NUMBER (14) PPG-411

7. AUTHOR(s) (10)
Viktor K. Decy, G. M. Morales, J. M. Dawson

8. CONTRACT OR GRANT NUMBER(s) (15) N00014-75-C-0476

9. PERFORMING ORGANIZATION NAME AND ADDRESS
Department of Physics
University of California
Los Angeles, California 90024

10. PROGRAM ELEMENT, PROJECT, TASK AREA & WORK UNIT NUMBERS

11. CONTROLLING OFFICE NAME AND ADDRESS
ONR
Physics Program Offic
Arlington, Virginia 22217

12. REPORT DATE (11) May 1979

13. NUMBER OF PAGES
36

14. MONITORING AGENCY NAME & ADDRESS(if different from Controlling Office)
Plasma Physics Group = PPG

15. SECURITY CLASS. (of this report)

15a. DECLASSIFICATION/DOWNGRADING SCHEDULE

16. DISTRIBUTION STATEMENT (of this Report)
Approved for public release; distribution unlimited.
(12) 40p.

DDC RECEIVED JUN 27 1979 C

17. DISTRIBUTION STATEMENT (of the abstract entered in Block 20, if different from Report)

18. SUPPLEMENTARY NOTES

19. KEY WORDS (Continue on reverse side if necessary and identify by block number)
Plasma Heating

20. ABSTRACT
A computer simulation study of the excitation of lower hybrid waves by external sources and the associated plasma heating is presented. A plasma slab with a nonuniform density profile is modeled with a 2 1/2 dimensional electrostatic particle code. Both a finite-length electrostatic antenna and a single wave exciter are considered. The frequency is chosen so that a wave conversion layer exists in the plasma. It is found that a narrow sheath is formed at the plasma edge and the dominant effect is surface electron heating within that region. Ponderomotive force effects as well as the nonlinear generation of harmonics and subharmonics also occur. A low amplitude lower hybrid wave is observed to be excited by the sources and propagates to the wave conversion layer where it is absorbed.

DD FORM 1 JAN 73 1473 EDITION OF 1 NOV 65 IS OBSOLETE
S/N 0102-LF-014-6601

SECURITY CLASSIFICATION OF THIS PAGE (When Data Entered)

401733

SIMULATION OF LOWER-HYBRID HEATING IN A NONUNIFORM PLASMA SLAB

Viktor K. Decyk, G. J. Morales, J. M. Dawson

PPG-411 May, 1979

Center for Plasma Physics and Fusion Engineering
University of California
Los Angeles, CA 90024

Abstract

A computer simulation study of the excitation of lower hybrid waves by external sources and the associated plasma heating is presented. A plasma slab with a nonuniform density profile is modeled with a 2 1/2 dimensional electrostatic particle code. Both a finite-length electrostatic antenna and a single wave exciter are considered. The frequency is chosen so that a wave conversion layer exists in the plasma. It is found that a narrow sheath is formed at the plasma edge and the dominant effect is surface electron heating within that region. Ponderomotive force effects as well as the nonlinear generation of harmonics and subharmonics also occur. A low amplitude lower hybrid wave is observed to be excited by the sources and propagates to the wave conversion layer where it is absorbed.

Accession For
NTIS GRA&I
DDC TAB
Unannounced
Justification
By
Distribution/
Availability Codes
Dist | Avail and/or special
A

I. Introduction

At the present time there exists plans throughout the world for high power plasma heating experiments using lower hybrid waves. This heating scheme has been extensively studied for more than a decade, and the present consensus is that this is a difficult problem, both from the experimental and theoretical standpoints. The problem involves strong surface nonlinearities due to the large electric fields expected, and the complications of device geometry and plasma inhomogeneities make the study of wave propagation rather complex even in the linear regime.

Computer simulation can be a useful tool in understanding some physics details that are part of the overall scheme, especially those aspects which are difficult to treat analytically. However, to do this economically with present day computers one must idealize the geometry and reduce the scale lengths to manageable proportions. Simulation thus provides a restricted but detailed view of the problem. In the work presented in this paper, the computer model calculates the self-consistent particle trajectories of electrons and ions in a magnetized slab geometry and provides a complete picture of the dynamics over a short time scale.

In a previous paper,[1] we examined the excitation of lower hybrid waves and their propagation in a homogeneous slab and focused our attention on the coupling to bounded plasma resources. For the lower hybrid heating scheme however, the plasma density nonuniformity plays an essential role. In general, the density nonuniformity gives rise to much richer phenomena than is allowed in the uniform case previously studied.[1] In particular, one is interested in the case in which the plasma contains a resonance layer for the RF frequency used. The study presented here is therefore a step closer to the

experimentally relevant situation. One other particle simulation on this topic has been reported.[2] However, some of their heating results are different from those in the present study. For the plasma parameters used in that work $\omega/\Omega_i \simeq 3$, and thus direct ion cyclotron damping was important.

The paper is organized as follows: Section II contains a discussion of the computer model and of the choice of parameters used in the simulation. In Sec. II, we discuss the wave excitation and plasma heating with a finite length source. The main effect observed is that most of the energy is deposited at the plasma surface and that a broad spectrum of harmonics is nonlinearly generated. A low amplitude lower hybrid wave is observed to propagate to the resonance layer and is absorbed. In Sec. IV, the case of a single k exciter is discussed. Finally, a summary is contained in Sec. V.

II. Computer Model

An electrostatic particle simulation model, described in detail elsewhere,[3] has been developed for this study and pertinent details are briefly summarized here. The model is bounded and is 2½ dimensional, i.e., the field quantities and particle positions are two dimensional, while all three velocity components are retained in the particle orbits. The fields are periodic in the direction of the external magnetic field ($\hat{z}$) and bounded in the perpendicular direction ($\hat{x}$). Finite-sized (Gaussian) particles are used throughout.

For the simulation results presented here, vacuum boundary conditions (i.e., no charges exist outside the slab boundary) are imposed in the $\hat{x}$ direction at x = 0. By imposing symmetry about the plane of maximum density, one needs to consider only half the physical length $2L_x$ in the x direction, reducing the computational effort. Such a boundary condition, obtained by requiring the normal electric field to vanish at $x = L_x$, is "transparent", i.e., one avoids boundary effects such as sheaths and surface waves. The physical consequences of this boundary condition are readily understandable in terms of equivalent image charges on the other side of the plane of symmetry. External sources, described later, are specified at x = 0, and due to symmetry, there is an equivalent image souce at $x = 2L_x$.

The choice of orientation of the magnetic field $\vec{B}_o$, which is constant in magnitude, means that while plasma drifts such as the $\vec{E} \times \vec{B}$ drift and diamagnetic drifts do occur in the model, their direction is in the third dimension ($\hat{y}$) and therefore they cannot couple with any electric fields. This configuration is useful for a first study, since it allows one to isolate the propagation of lower hybrid waves and plasma heating without the complications

due to parametric effects driven by $\vec{E} \times \vec{B}$ drifts and scattering by drift waves, which are not permitted to occur in this geometry. In a future study, these effects will be considered by tilting the direction of the magnetic field in the yz plane.

The initial plasma density is taken to be uniform in the $\hat{z}$ direction and inhomogeneous in $\hat{x}$, so that $\nabla n \perp \vec{B}o$. The density has its minimum value at the vacuum boundary (x = 0) and increases monotonically to a maximum value at the symmetry plane $x = L_x$ (with $n_{max}/n_{min} = 10$), according to the general form:

$$n(x) = \bar{n} \{\beta + \lambda \exp [- (x - L_x)^2/2\alpha^2]\}, \qquad (1)$$

where $\bar{n}$ is the average plasma density, defined as the ratio of the total number of particles in the simulation by the plasma area. The initial temperature profiles are uniform in space with $T_e/T_i = 10$. The initial electron thermal velocity was chosen to be $v_{the} = 0.7\delta\ \bar{\omega}_{pe}$, where δ is the distance between grid points used in the simulation, and $\bar{\omega}_{pe}$ is the average plasma frequency, $\bar{\omega}_{pe} \equiv (4\pi\bar{n}e^2/m_e)^{\frac{1}{2}}$. The dimensionless average Debye length $\bar{\lambda}_{De}$ which will appear in later expressions then has the value 0.7.

Each finite-size particle has a distribution of charge given by: $\rho(\vec{r}_j) = \frac{q_j}{2\pi a^2} \exp [- (\vec{r} - \vec{r}_j)^2/2a^2]$, where $a = .8\delta$. The ratio of the electron cyclotron to average plasma frequency is $\Omega_e/\bar{\omega}_{pe} = 1.5$, and the ion-electron mass ratio is $M_i/m_e = 50$. This then gives an initial ion Larmor radius $\rho_i \equiv v_{thi}/\Omega_i = 1.04\delta$. Particles are reflected elastically at both boundaries, with the full dynamics calculated correctly to second order in the time step $\Delta t = 0.2\ \bar{\omega}_{pe}^{-1}$. The reflection of particles implies there is no

mechanism for net energy loss in the system. The number of grid points used is $L_x/\delta = 64$ and $L_z/\delta = 128$.

The external source in these simulations is determined by specifying an external surface charge density oscillating with a specified frequency ω_o on the boundary of the slab. Because the magnitude of the charge density is fixed externally, such a source corresponds to a constant current driver. The phase of the oscillator is chosen so that the field is zero at $t = 0$ (i.e., a quasi-adiabatic turn on).

Energy conservation was checked by calculating the work done by the external source and subtracting this value from the total plasma energy. In all cases, energy is conserved to within 3%.

III. Coupling by a Short Capacitor Plate Antenna

In the geometry outlined in the previous section, the lower hybrid waves of interest have a finite but small wavenumber $k_{\parallel}$ along $\vec{B}_o$. Since the system is periodic in $\hat{z}$, the wavenumbers in that direction are quantized according to $k_{\parallel} = k_m = 2m\pi/L_z$, where m is an integer (mode number). In the perpendicular ($\hat{x}$) direction, the wavenumber $k_{\perp}$ is not constant because the plasma density varies with position according to Eq.(1). In the cold plasma limit, electrostatic lower hybrid waves can reach the resonance layer ($k_{\perp} \to \infty$), where the frequency ω of the wave equals the lower hybrid frequency ω_{LH}, defined by

$$\omega^2_{LH} = \omega^2_{pi}/(1 + \omega_{pe}{}^2/\Omega_e{}^2). \tag{2}$$

However, finite temperature effects introduce an additional mode of oscillation and instead of a resonance, one encounters a wave conversion layer where two roots of the dispersion relation coalesce and $k_{\perp}$ becomes complex. The lower

hybrid heating scheme is based on the idea that the mode converted wave can be efficiently damped by plasma ions.

Using a warm electron-cold ion fluid model,[4] one can calculate the position of the wave conversion layer for the density profile used, Eq. (1). The result of the calculation is shown by the curves labeled ω_m (m = 1, 2) in Fig. 1. Each of these curves represents the location of the layer for the mode number m as a function of frequency. One finds that ω_m is bounded by $\omega_{LH} < \omega_m < (\omega_{pi}^2 + \Omega_i^2)^{\frac{1}{2}}$, and these upper and lower bounds, along with the density profile n(x) are also shown in Fig. 1. The frequency of the source ω_o is chosen for practical reasons to be $\omega_o/\omega_{pe} = 0.14$, which gives a wave conversion layer for mode m = 1 about 2/3 of the way inside the plasma, as indicated by the dashed line in Fig. 1.

Two capacitor plates of finite length, oscillating out of phase, are chosen as the coupler structure. The vacuum equipotential lines generated by this source are shown in Fig. 2(a). The wavenumber spectrum of this source, illustrated in Fig. 2(b), is a broad-band spectrum peaked at mode m = 3 (with parallel phase velocity $\omega_o/k_m = 1.4\ v_{the}$). The magnitude of the surface charge density σ on each plate is fixed to be $e\sigma/kT_e = 0.57\delta^{-1}$. This source creates an electric field at the boundary whose maximum amplitude is (in vacuum)

$$\frac{|E|^2}{8\pi\bar{n}\kappa T_e} = 14.6. \tag{3}$$

When integrated over the plasma volume, the total field energy of the source (in vacuum) is close to 7% of the total electron kinetic energy at t = 0.

The system is followed for about 11 oscillation periods of the source. The total electric field energy (w_{ef}), shown in Fig. 3, shows no growth in

time, as when one excites a bounded plasma resonance.[1] The energies in the simulation are normalized to the initial total electron thermal energy, i.e.,

$$w_{ef} \equiv \frac{1}{\frac{3}{2}N_p \kappa T_e} \int \frac{E^2}{8\pi} \, dA \tag{4}$$

for the electric field energy, where $N_p = 17280$ is the number of electrons in the simulation. The kinetic energy of species α is normalized in an analogous manner:

$$w_\alpha \equiv \frac{1}{3N_p \kappa T_e} \, m_\alpha \sum_j v_j^2 . \tag{5}$$

The electron kinetic energy (w_e), shown in Fig. 4, increases rapidly at first, and then grows at a slower rate, while the ion kinetic energy (w_i) shows a secular increase. At the end of the simulation, the total plasma energy increased by 35%, with 55% of this energy gain going to the electrons and 45% to the ions. The details of this energy partition are discussed in the next section.

Because lower hybrid waves were only weakly excited, two-dimensional interferograms were made to observe the space-time evolution of the plasma response clearly. These are essentially correlations between the external source and the plasma potential $\Phi(x,y)$ defined by:

$$\phi(x,y,\tau) \equiv \frac{1}{T} \int_0^T \sin(\omega_o t) \, \Phi(x,y,t+\tau) dt. \tag{6}$$

The length of integration T must be long enough to resolve the frequency ω_o, but not so long that slow changes in the zero order plasma properties are included. Such an interferogram is shown in Fig. 5, for $\tau = 0$. The most striking feature in this diagram is the large potential drop at the

edge, i.e., the plasma forms a sheath which shields out the external fields. A much less evident feature (due to the scale normalization) is the low amplitude lower hybrid wave which is being excited. It is more easily seen in the equipotential plot inserted in Fig. 5. The well-known resonance cones predicted from cold plasma theory were not observed in this case (although they have been seen in our earlier studies[1]), because only a single mode penetrates deep into the plasma. A Fourier analysis of the pattern shown in Fig. 5 in the periodic direction shows (Fig. 6) that mode m = 1 is the only one which significantly penetrates into the plasma, because its phase velocity ($\omega_o/k_m = 4.1\ v_{the}$) is the only one large enough that it is not subject to strong electron Landau damping. Although the source had a broad-band spectrum of modes (Fig. 2b), the plasma surface acts as a "filter" which transforms the spectrum into a single mode. This single mode propagates to the wave conversion layer, which is indicated by the arrow in Fig. 6.

From these observations one concludes that there are two distinct regions where different plasma behavior takes place. First there is the sheath region around the source, where large electric fields are present and non-linear phenomena are expected to be important. Secondly, in the plasma interior, there is a low amplitude lower hybrid wave which propagates toward a mode conversion layer, where the plasma properties remain essentially linear. In the following subsections we examine the physics of these two regions separately.

A. Sheath region

The dominant effect which occurs in this region ($0 \lesssim x \lesssim 16$) is large electron surface heating, as is expected due to the large amplitude of the electric fields and the shape of the spectrum. The time evolution of the electron velocity distribution function in the parallel direction $f_e(v_{\parallel})$ in this region first shows electrons quickly being pulled into the tails of the distribution within $1\frac{1}{2}$ oscillation periods of the source. The total electron kinetic energy (Fig. 4) shows a corresponding rapid rise. On a longer time scale, particles initially in the bulk of the distribution, also gain energy, but now at a linear rate given by $\frac{1}{\omega_{pe}} \frac{dw_e}{dt} \simeq 2.7 \times 10^{-4}$, and the energy shown in Fig. 4 reflects this. By the end of the simulation, the plasma distribution function for electrons near the edge (Fig. 7) is approximately a bi-Maxwellian, where the majority ($\simeq$60%) of the electrons have an effective temperature which is approximately ten times hotter than the temperature of the background (40%). Figure 8 shows the spatial dependence (perpendicular to $\vec{B}_o$) of the electron kinetic energy w_e, normalized to the local plasma density n_e; clearly, the electron energy gain is localized to the edge region.

Except for the initial transients, the heating process here is best described by the term transit-time heating.[5-7] When electrons transist through a localized region of oscillating electric field with random phases relative to the rf, some particles gain a velocity increment Δv, while the velocity of an equal number is decreased by Δv. However, the energy gain of particles with $\Delta v > 0$ is larger than the energy loss of those with $\Delta v < 0$, and thus the energy of a distribution of particles will on the average increase. The theoretical rate of energy increase for a 1-D system, where $\Delta v \ll v_{th}$, has been shown to be linear in time,[5, 6] which is in agreement with the simulation results. However, the parameters in the simulation were such

that at the surface $\Delta v_{max} = \frac{qE_o}{m\omega_o} \sim 5\, v_{the}$, which is not the regime assumed by the theoretical expressions.

Due to the presence of large localized electric fields at the surface, one expects that ponderomotive force effects should play a role. This effect is evident in Fig. 9, where contour lines of constant density are plotted. (The density is time-averaged over the interval $100 < \omega_{pe} t < 500$). One can see that near the antenna, the plasma has been expelled and a density cavity formed ($\delta n_e / n_e \lesssim 30\%$). The ions also increase their kinetic energy in the region near the antenna, due to the direct acceleration by the source field. Ions which acquire a large perpendicular velocity now have large Larmor radii, and they migrate into the plasma interior. This surface ion heating will be discussed in more detail in a later section.

In summary, one attains a plasma at the edge whose electron temperature is ten times hotter and in which a density cavity forms around the antenna due to the ponderomotive force. These changes at the edge then modify the manner in which the ideal capacitor plate antenna couples the external RF energy to the plasma interior.

B. Spectral Broadening

Another important feature which has its origin in the sheath region is the generation of a broad frequency spectrum which includes harmonics and subharmonics of the external excitation frequency ω_o. In Fig. 10, we show a power spectrum for mode $m = 1$ at various points in space, defined by

$$P_m(x,\omega) \equiv \frac{\tilde{\lambda}_{De}^2}{4\pi \bar{n}_o \kappa T_e} |\vec{E}_m(x,\omega)|^2. \qquad (7)$$

One finds that the driving frequency ω_o is the dominant feature in the spectrum for those values of x such that $\omega_o \lesssim \omega_{LH}(x)$, i.e., below its cut-off point at the wave conversion layer at $x \simeq 40$. In addition, one finds ion cyclotron modulation which is evident in the generation of upper and lower side-bands $\omega \approx \omega_o \pm \Omega_i$. Since the lower side-band is cut off at a location given by $\omega_o - \Omega_i \simeq \omega_{LH}(x) < \omega_o$ (i.e., at $x \simeq 24$), it does not penetrate deep into the interior; however, the upper sideband penetrates deeper than the fundamental wave launched by the antenna (e.g., at x = 48). This ion cyclotron modulation is a phenomena which we observed in our earlier study whenever finite-size antennae were used.

Another frequency seen near the sheath region ($x \lesssim 12$) in Fig. 10 is the half-harmonic $\omega_o/2$. It turns out that the local lower hybrid frequency near the antenna is approximately equal to $\omega_o/2$. A plasma oscillation at $\omega_o/2$ is found to be excited and driven to large amplitude near the density depression created by the ponderomotive force (Fig. 9). This excitation process is an example of the classic parametric excitation described by Mathieu's equation:

$$\frac{d^2x}{dt^2} + \Omega_o^2[1 + \varepsilon \cos \omega_o t]x = 0 \qquad (8)$$

when a normal mode frequency is modulated by an external source.[8, 9] This model equation predicts that when $\omega_o \simeq 2\Omega_o$ odd numbered harmonics of $\omega_o/2$ would also be excited, e.g., $3\omega_o/2$ arises due to the non-linear mixing

of $\omega_o/2$ with the fundamental ω_o. In Fig. 10, one indeed sees peaks at $3\omega_o/2$, $5\omega_o/2$ and $7\omega_o/2$. Finally, the first harmonic at $2\omega_o$ is also seen in Fig. 10, corresponding to the non-linear mixing of the fundamental with itself. One can estimate from Fig. 10 that the power in the harmonics is an order of magnitude smaller than the power at ω_o.

Harmonics at other mode numbers (m = 0, 2) were also observed. For mode m = 2, we find that a peak at $\omega = \omega_o$ exists only near the sheath region because $\omega_o/k_{\parallel} = 2.0\ v_{the}$ for this mode, as expected from Fig. 6. However, the first harmonic $\omega = 2\omega_o$ is found in the plasma interior because it has a phase velocity ($2\omega_o/k_{\parallel} = 4.1\ v_{the}$) in excess of the electron thermal velocity and is not subject to strong Landau damping. The frequencies $\omega_o/2$, $3\omega_o/2$ and $5\omega_o/2$ were also observed for this mode.

C. Wave Propagation in the Plasma Interior

Wave propatation characteristics can be extracted by introducing a lag time τ in the interferogram defined by Eq. 6. In Fig. 11, we examine the propagation of the dominant mode m = 1, by showing the spatial dependence of the potential at succeeding lag times. One can see that the phase fronts are propagating toward the antenna. Since lower hybrid waves have oppositely directed group and phase velocities, this confirms that the direction of energy flow is toward the interior. The wave propagates toward the wave conversion layer with diminishing amplitude until it is totally absorbed.

To examine more carefully whether any wave conversion to short wavelength ion waves occurs as the wave approaches the center of the plasma, we show in Fig. 12, the interferograms of the ion density $\tilde{n}_m^i(x,\tau)$, defined in analogy to Eq. 6. First, one sees that the ions contribute to the lower hybrid wave only when the density is sufficiently large ($x \gtrsim 30$, $\omega_o \lesssim \omega_{LH}$). When the

density is low, the lower hybrid wave is predominantly an electron wave. In the high density regions, where the ions are contributing to the lower hybrid wave, one finds that the phase fronts are moving in the $-\hat{x}$ direction, with the same wavelength as in Fig. 11. Since no appreciable standing wave pattern is observed, one can conclude (to within 10%) that neither reflection, nor transmission from the image source at $x = 2L_x$ (due to the use of symmetric boundary conditions) has occurred. The conclusion is that the wave is totally absorbed with no measurable wave conversion.

In spite of the fact that the wave is totally absorbed, it is difficult to show any corresponding increase in particle kinetic energy, since the wave amplitude is so low (only a few times the thermal noise level) and other effects, such as heat exchange due to collisions between the initially hot electrons and the cold ions, are more important.

IV. Lower Hybrid Waves Driven by Single k Exciter

In order to excite the lower hybrid wave more efficiently, we chose an external source where the energy would be predominantly in the mode $m = 1$. The geometry consisted of two capacitor plates each of length $L_z/2$. The amplitude was chosen ($e\sigma/\kappa T_e = .18\delta^{-1}$) so that the total energy of the source (in vacuum) was the same as the previous case, but concentrated primarily in a single mode. All the other simulation parameters remained the same.

The two dimensional interferogram (Fig. 13) for this case shows that although the structure of the sheath has changed, the low amplitude lower hybrid wave excited in the plasma interior looks much the same as before, with about a factor of two increase in amplitude. The major difference from the previous case was in the properties of the sheath region.

The kinetic energy of each species as a function of time is shown in Fig. 14. One can see that while the electron kinetic energy gain was more than double the previous case, the ion energy gain was about the same. As mentioned previously, the ions gain energy by being accelerated directly by the source fields. This effect is illustrated in the phase-space diagram in Fig. 15, where we plot the co-ordinates (x, v_x) for all the ions. One finds a small population of ions being accelerated from the source at $x = 0$ to velocities as large as fifteen times the ion thermal velocity, and penetrating to the plasma interior. (In a real experiment, of course, many of the ions would be lost in the system, whereas in this computer experiment the ions are reflected if they reach the boundary). Figure 16 shows the spatial distribution of the ion kinetic energy density in this case.

There were fewer harmonics generated with this source. For mode $m = 1$, the ion cyclotron modulation was absent, and the $\omega_o/2$ excitation was much weaker. The first harmonic $2\omega_o$ was also present. For mode $m = 2$, the main effect was an oscillation with $(2\omega_o, 2k_o)$, since no power was being supplied by the source at that wave number. There is thus an effective up-shifting of the wavenumber spectrum due to the non-linearities in the sheath.

The wave propagation characteristics of the fundamental in this case were the same as those shown in Fig. 11.

V. Conclusion

In all RF heating experiments one must contend with sheath regions around the antenna. Large amplitude sheaths are especially difficult to analyze and are poorly understood. In this simulation, we have demonstrated that for electrostatic excitation, such sheaths play an important role in the efficiency of excitation and the power absorption. Further simulation can shed much light on this complex problem.

To summarize the results, with electrostatic antennae of the type used here, most of the energy lies within a narrow sheath region at the edge. Only modes with $\omega_o/k_{\parallel} \gtrsim 2.5\ v_{the}$ are excited in the plasma interior, and these have low amplitudes. The result is that the dominant effect is surface heating. The electrons at the surface absorb 55-75% of the total energy. Ions absorb most of the remainder at the surface and migrate toward the interior. For finite-sized antennae, a significant density depression ($\delta n/n \gtrsim 30\%$) is created in front of the source. This depression plays a role in some of the harmonics which are non-linearly generated. About 5% of the energy goes into a wide variety of harmonics, e.g., $\omega_o/2$, $3\omega_o/2$, $2\omega_o$. Ion cyclotron modulation at $\omega \simeq \omega_o \pm \Omega_i$ is observed whenever finite-size antenna were used. The low amplitude fundamental wave at ω_o is observed to propagate toward the interior, where it is absorbed.

ACKNOWLEDGMENTS

This work is supported by U-S D.O.E. Contract Number EY-76-C-03-0010 and the Office of Naval Research Contract Number ONR N00014-75-C-0476 P00004.

REFERENCES

1. V. K. Decyk, J. M. Dawson, and G. J. Morales, Phys. Fluids 22, 507 (1979)
2. Hirotada Abe, Hiroyuki Kajitani, and Ryohei Itatani, Nagoya University Institute of Plasma Physics Report IPPJ-296 (1977).
3. Viktor K. Decyk and John M. Dawson, J. Computational Phys., to be published
4. Viktor K. Decyk, Ph.D. dissertation, University of California, Los Angeles (1977).
5. G. J. Morales and Y. C. Lee, Phys. Rev. Lett. 33, 1534 (1974)
6. Hideo Sugai, Kazuo Ido, and Susumu Takeda, J. Phys. Soc. Japan 46, 228 (1979)
7. J. M. Berger, W. A. Newcomb, J. M. Dawson, E. A. Frieman, R. M. Kulsrud, and A. Lenard, Phys. Fludis 1, 301 (1958).
8. Mechanics by L. D. Landau and E. M. Lifshitz [Addison-Wesley, Reading, Mass., 1969], p.80.
9. Kyoji Nishikawa and C. S. Liu, Advances in Plasma Physics, vol 6, [John Wiley, New York, 1976], p.7.

FIGURE CAPTIONS

Fig. 1 Lower Hybrid wave conversion frequencies $\omega_m(x)$ for mode numbers m = 1, 2, the frequencies $\omega_{LH}(x)$ and $\sqrt{\omega_{pi}^2(x) + \Omega_i^2}$, for the initial density profile n (x). X is the co-ordinate perpendicular to the magnetic field. The driving frequency ω_o is chosen to give a wave conversion layer for m = 1 about 2/3 of the way inside the plasma.

Fig. 2 (a) Equipotential lines for finite-size exciter in vacuum.
(b) Wave number spectrum for finite-size exciter in vacuum. The small secondary peaks for large wavenumber are due to the sharp cutoff of the external charge distribution on the plates.

Fig. 3 Time evolution of the total electric field energy for the finite-size exciter case.

Fig. 4 Time evolution of the electron (w_e) and ion (w_i) kinetic energies for the finite-size exciter case. (Initial temperature ratio was $T_e/T_i = 10.$)

Fig. 5 Spatial dependence of the interferograms of the plasma potential (at $\tau = 0$) with equipotential plot inserted, showing the large sheath region around the antenna and the low amplitude lower hybrid waves, for finite-size exciter case.

Fig. 6 Interferograms of plasma potential (at $\tau = 0$) for Fourier modes m = 1,2, shown as a function of the perpendicular co-ordinate X. ($\tilde{\lambda}_{De} = .7$; solid line shows Im ϕ_m and dashed line shows Re ϕ_m).

Fig. 7 Electron velocity distribution parallel to the magnetic field for electrons near the edge region ($0 < x < 16$). (Dashed line shows initial distribution and solid line shows distribution at $\bar{\omega}_{pe}t = 480$).

Fig. 8 Spatial dependence perpendicular to $\vec{B}_o$ of the electron kinetic energy density at various times.

Fig. 9 Contour lines of constant values of the time averaged electron density n_e, illustrating the density cavity formed around the antenna.

Fig. 10 Power spectrum for Fourier mode m = 1 as a function of frequency at various spatial locations. ω_o is the externally excited mode.

Fig. 11 Interferograms of potential due to Fourier mode m = 1 as a function of the perpendicular co-ordinate at various lag times τ shows direction of wave-phase propagation corresponds to a backward wave.

Fig. 12 Interferograms of ion density for Fourier mode m = 1 as a function of the perpendicular co-ordinate at various lag times τ.

Fig. 13 Spatial dependence of the interferograms of the potential (at $\tau = 0$) with equipotential plot inserted, for single k exciter.

Fig. 14 Time evolution of the electron (w_e) and ion (w_i) kinetic energies for the single k exciter case. (Initial temperature ratio was $T_e/T_i = 10$).

Fig. 15 Ion phase space, showing the co-ordinates (x, v_x) of all the ions at time $\bar{\omega}_{pe}t = 100$.

Fig. 16 Spatial dependence perpendicular to $\vec{B}_o$ of the ion kinetic energy density at various times.

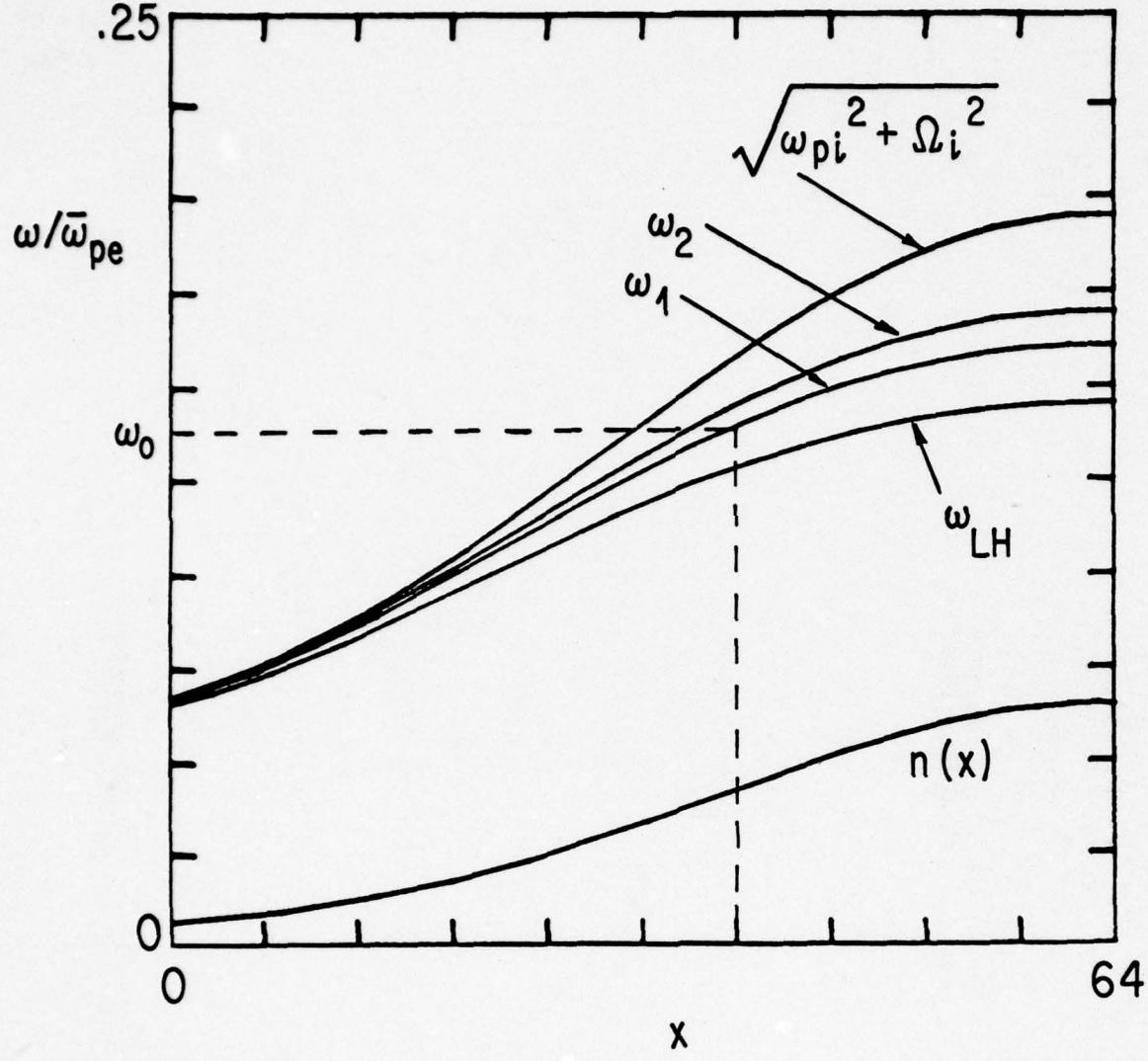
.25
$\omega/\bar{\omega}_{pe}$
$\sqrt{\omega_{pi}^2 + \Omega_i^2}$
ω_2
ω_1
ω_0
ω_{LH}
n(x)
0
0
64
X

FIGURE 1

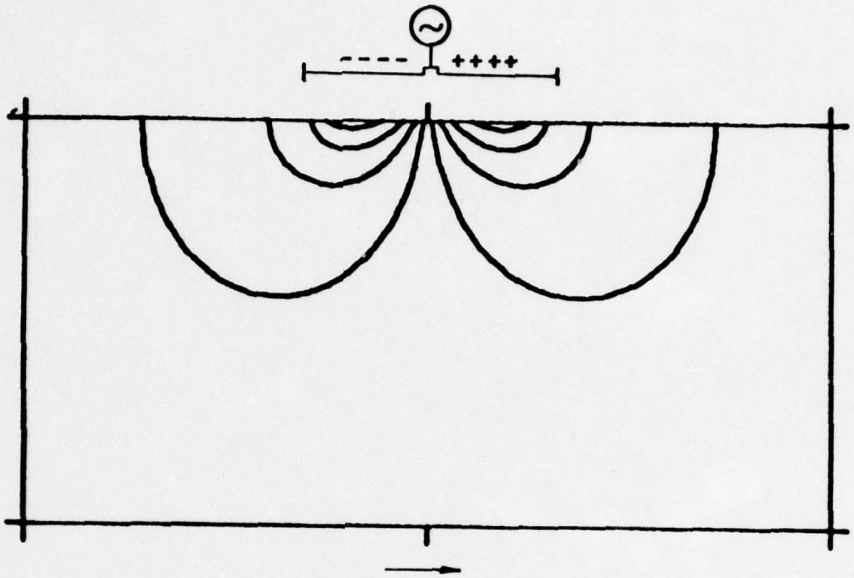

(a)

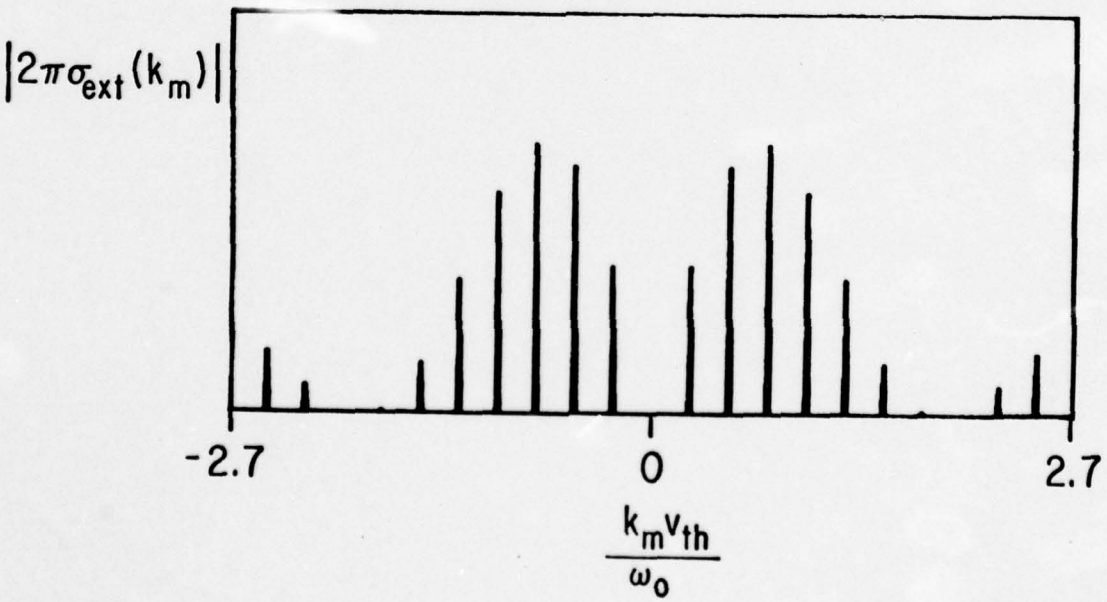

(b)

FIGURE 2

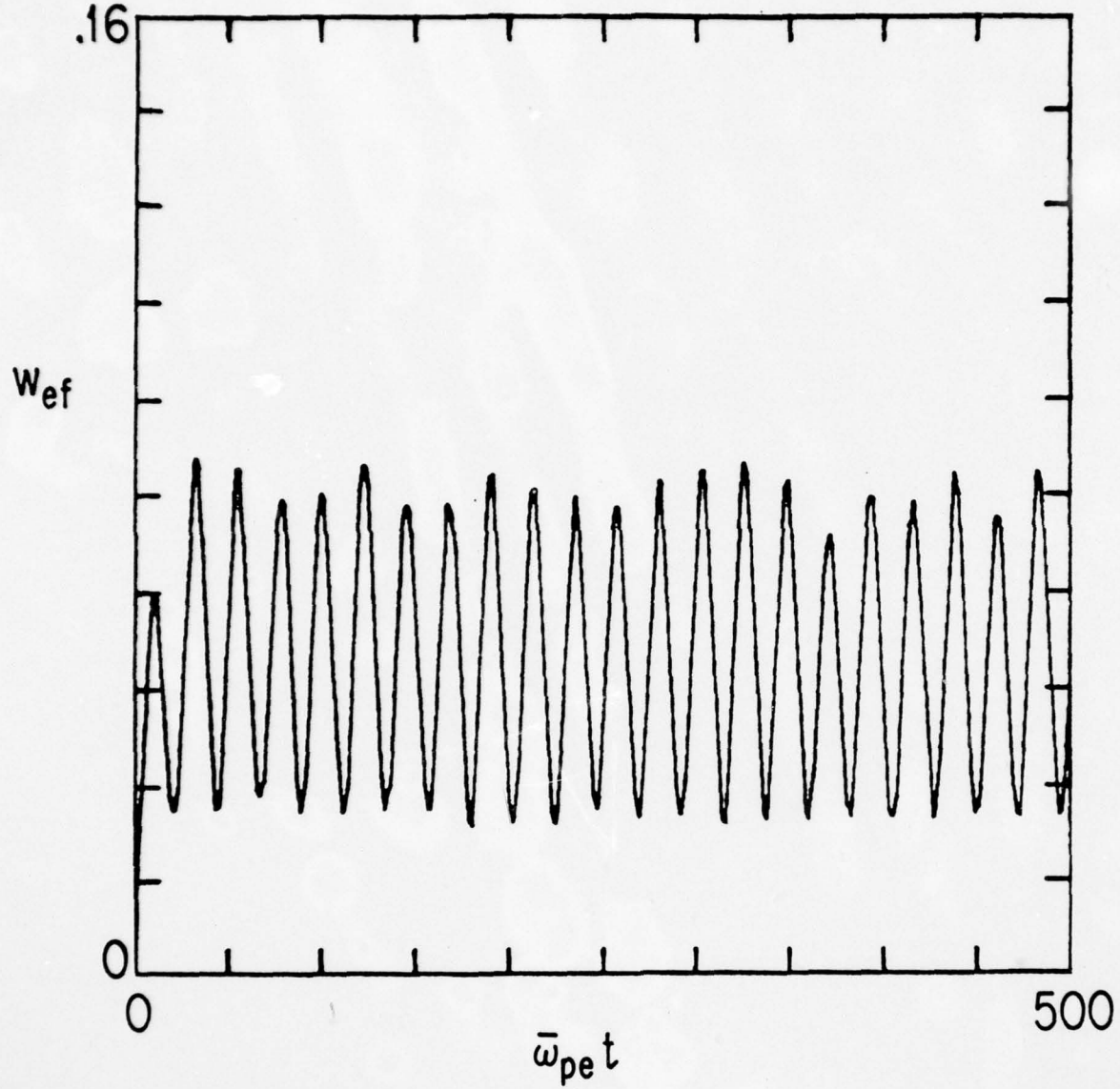

FIGURE 3

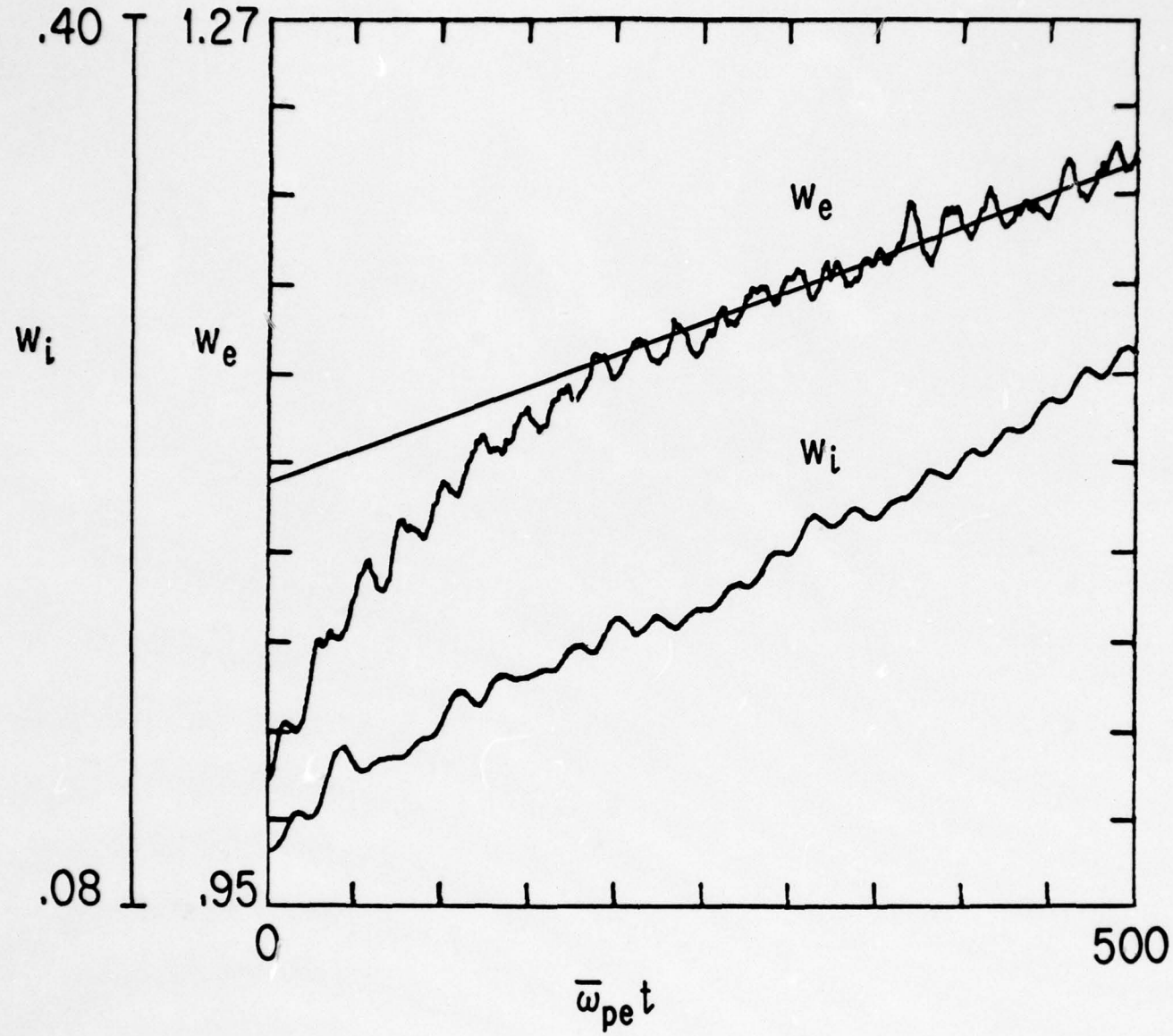

FIGURE 4

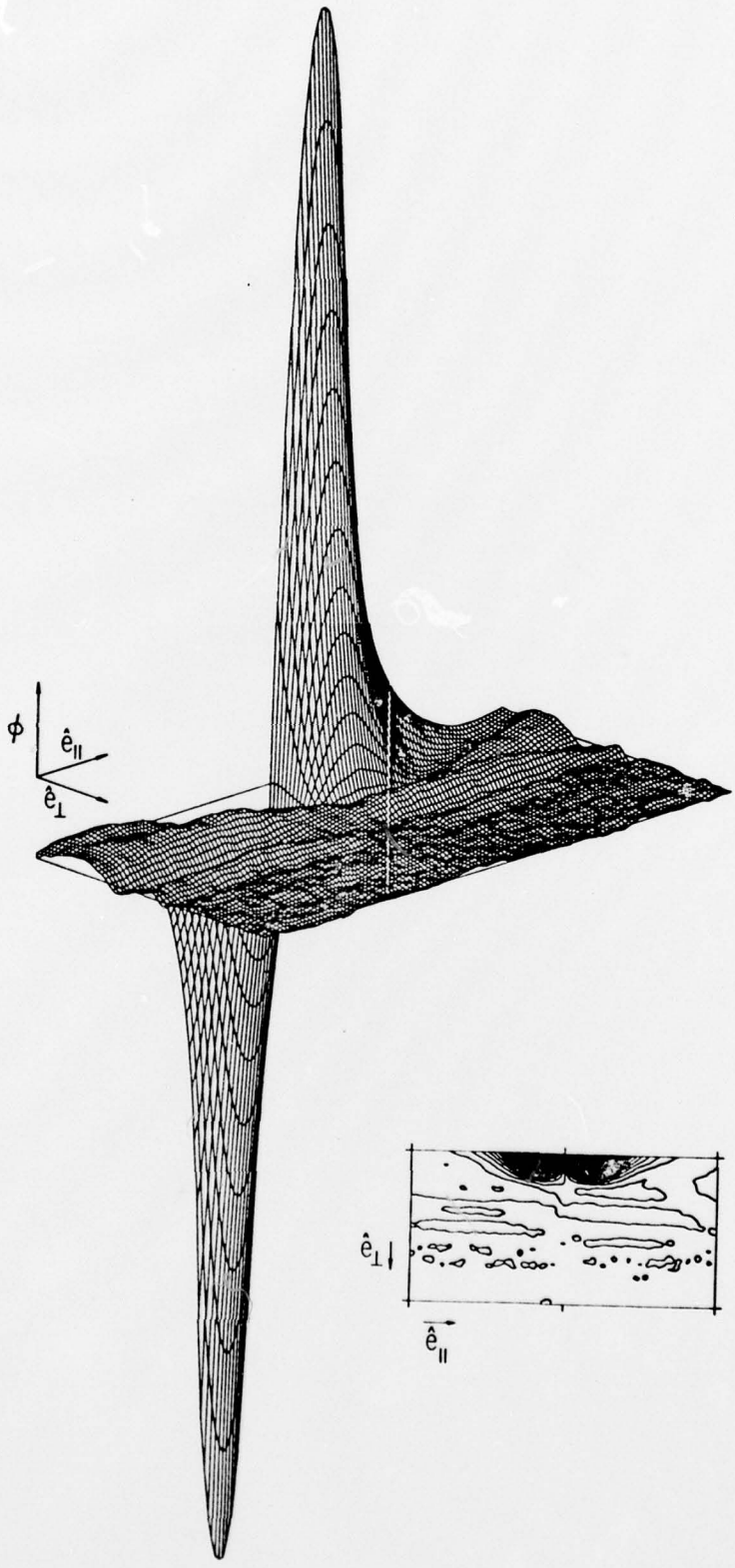

FIGURE 5

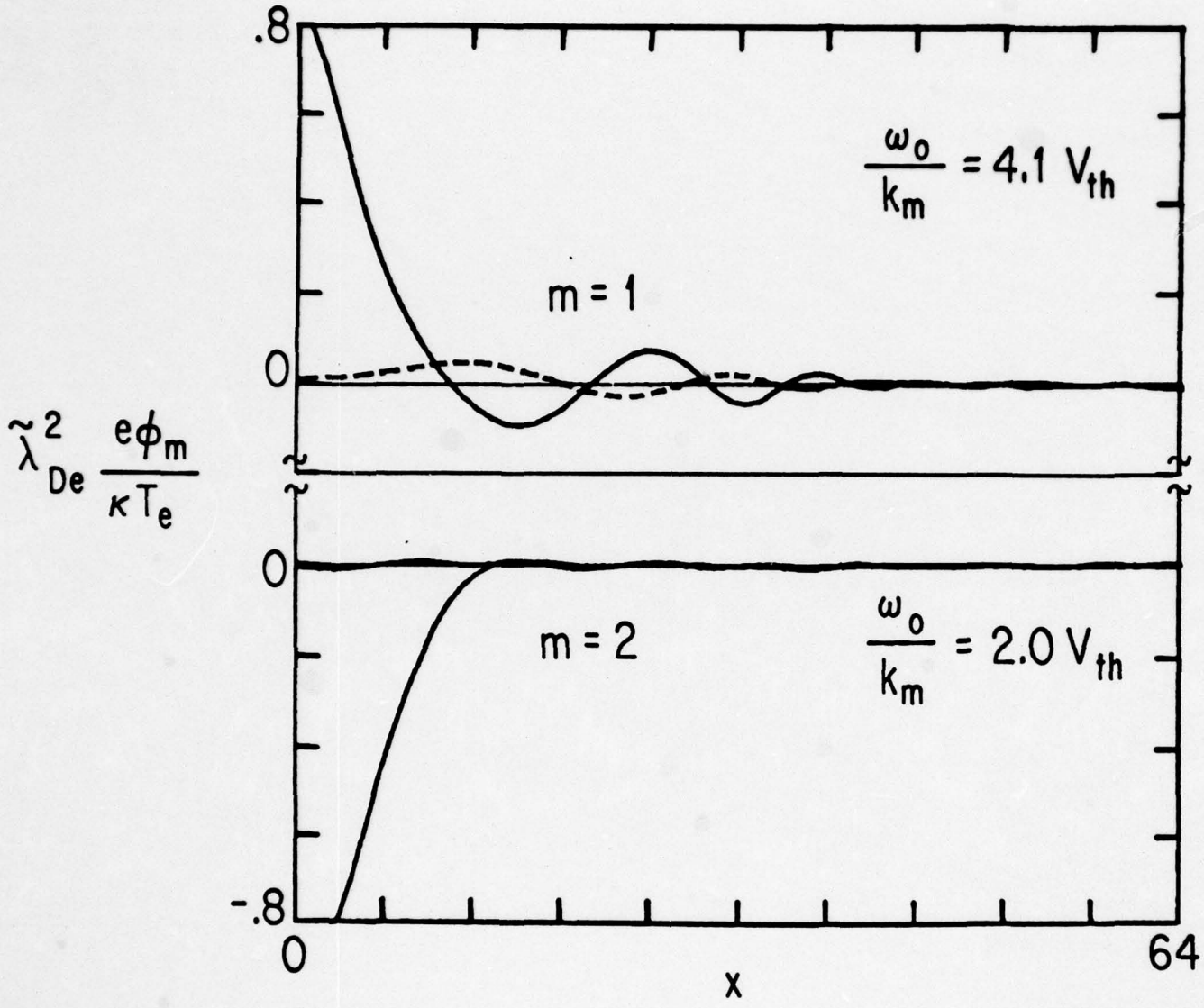
.8
0
0
-.8
0
64
x
$\tilde{\lambda}^2_{De} \frac{e\phi_m}{\kappa T_e}$
$\frac{\omega_o}{k_m} = 4.1\ V_{th}$
m = 1
m = 2
$\frac{\omega_o}{k_m} = 2.0\ V_{th}$

FIGURE 6

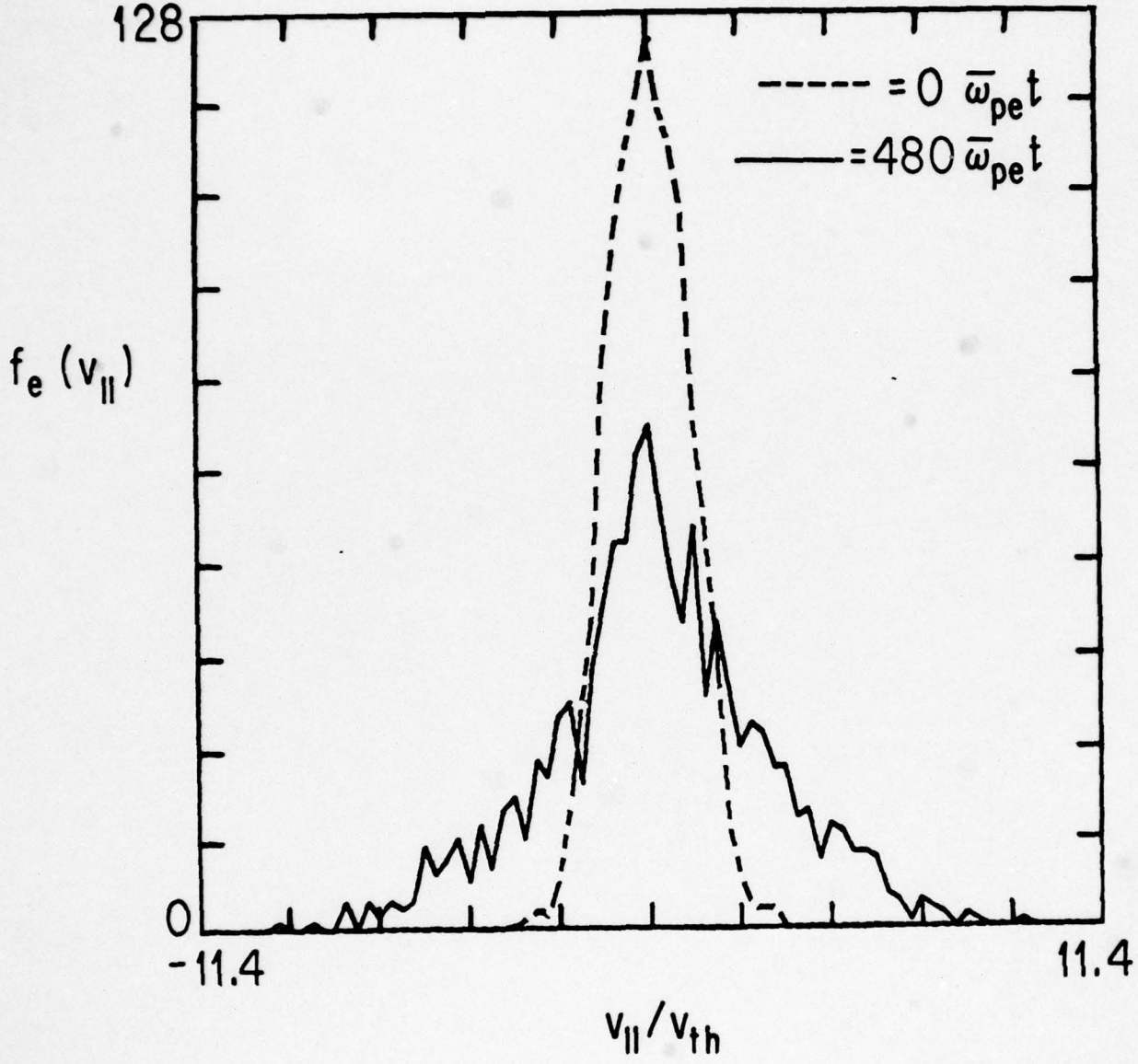

FIGURE 7

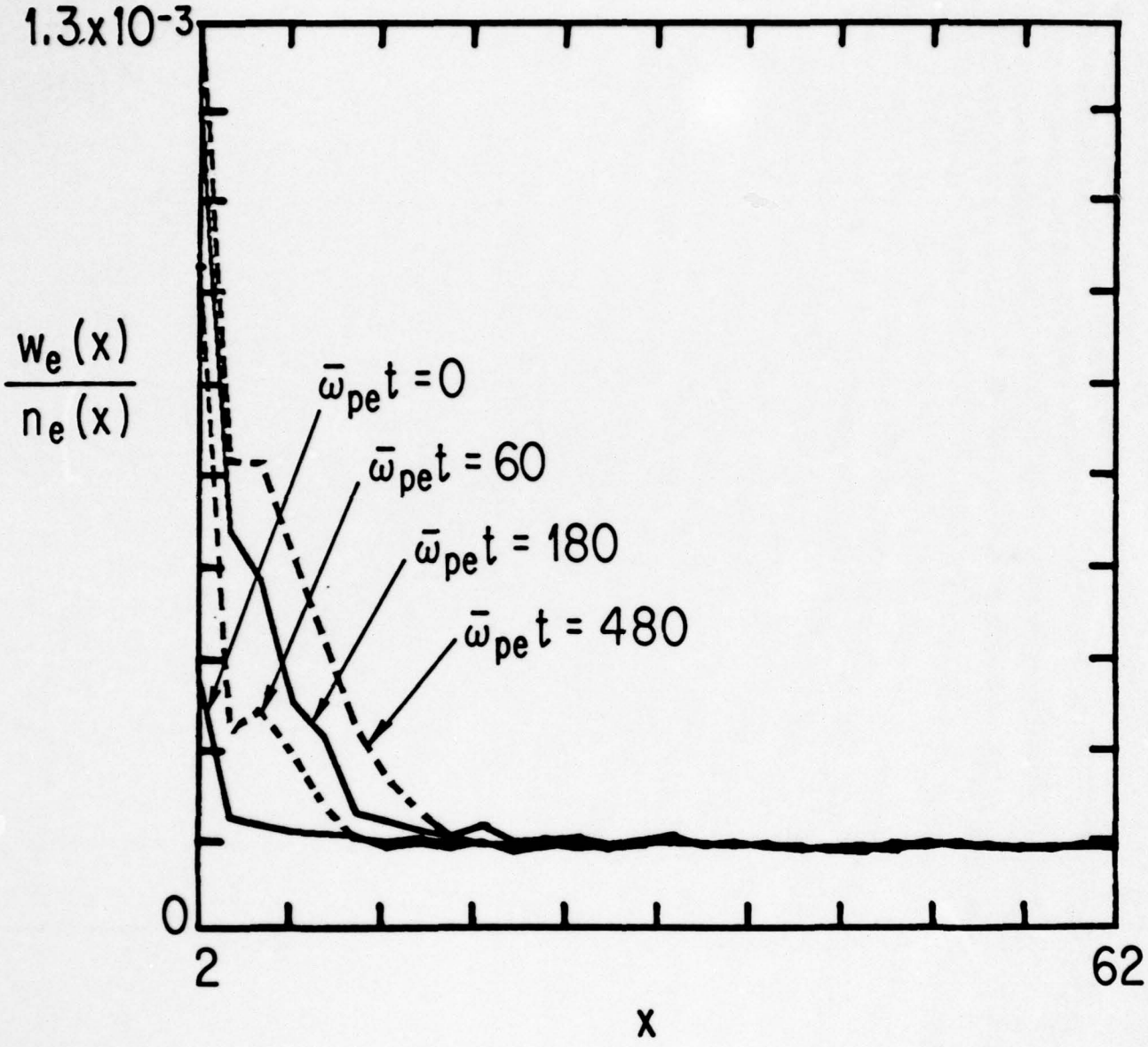
1.3x10⁻³
$\frac{w_e(x)}{n_e(x)}$
$\bar{\omega}_{pe}t = 0$
$\bar{\omega}_{pe}t = 60$
$\bar{\omega}_{pe}t = 180$
$\bar{\omega}_{pe}t = 480$
0
2
62
X

FIGURE 8

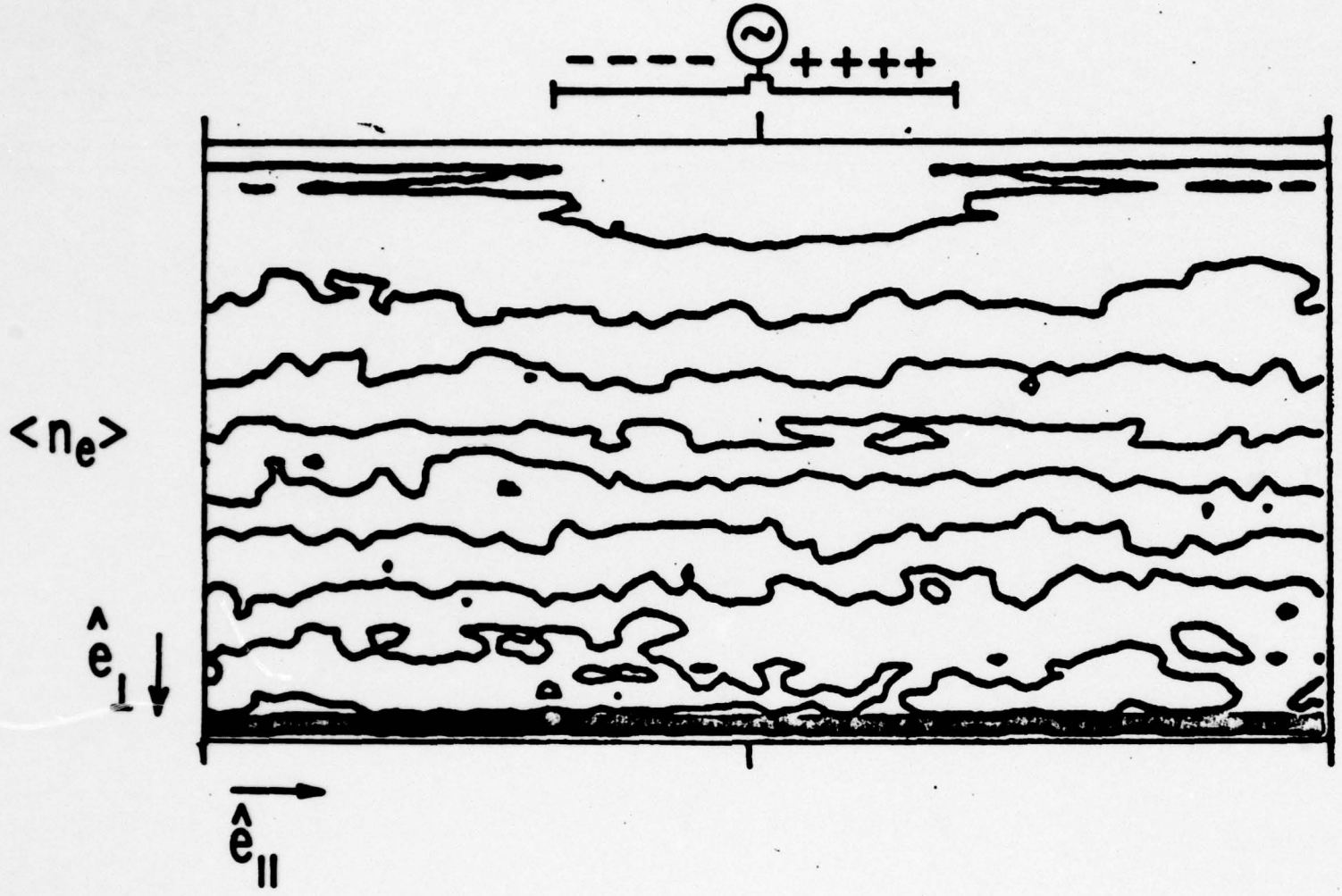

FIGURE 9

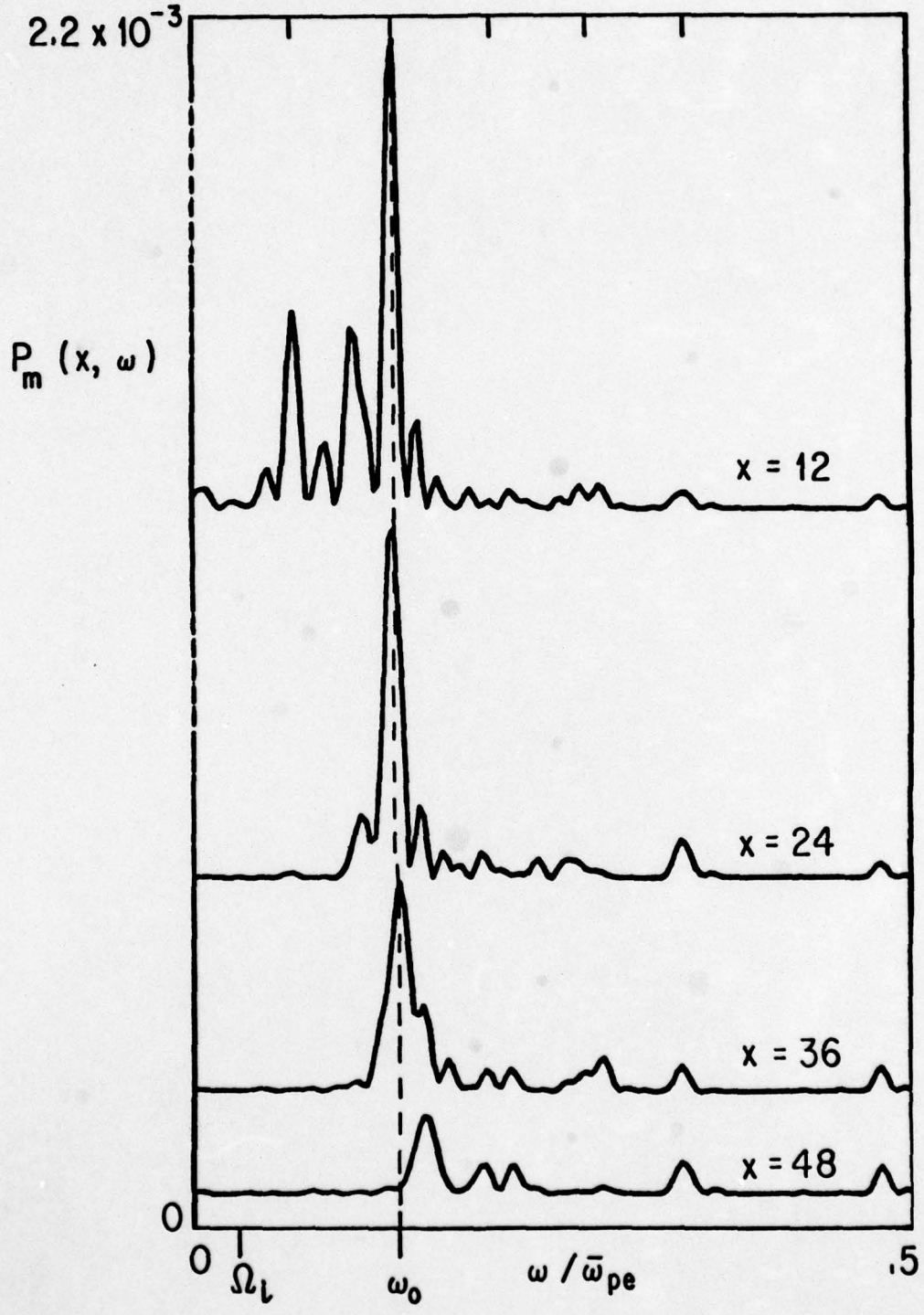

FIGURE 10

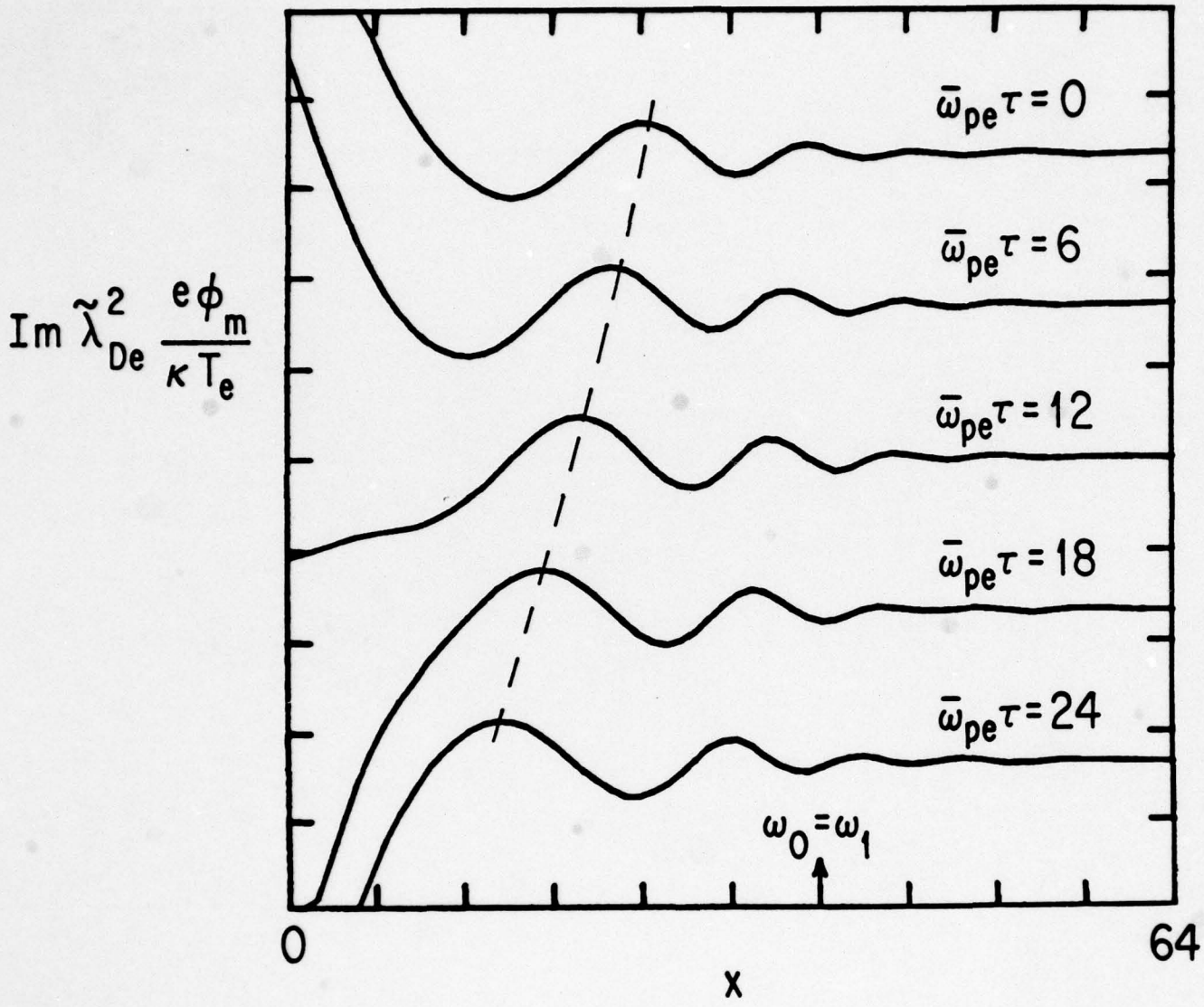
$\mathrm{Im}\,\tilde{\lambda}_{De}^2 \frac{e\phi_m}{\kappa T_e}$
$\bar{\omega}_{pe}\tau = 0$
$\bar{\omega}_{pe}\tau = 6$
$\bar{\omega}_{pe}\tau = 12$
$\bar{\omega}_{pe}\tau = 18$
$\bar{\omega}_{pe}\tau = 24$
$\omega_0 = \omega_1$
0
64
X

FIGURE 11

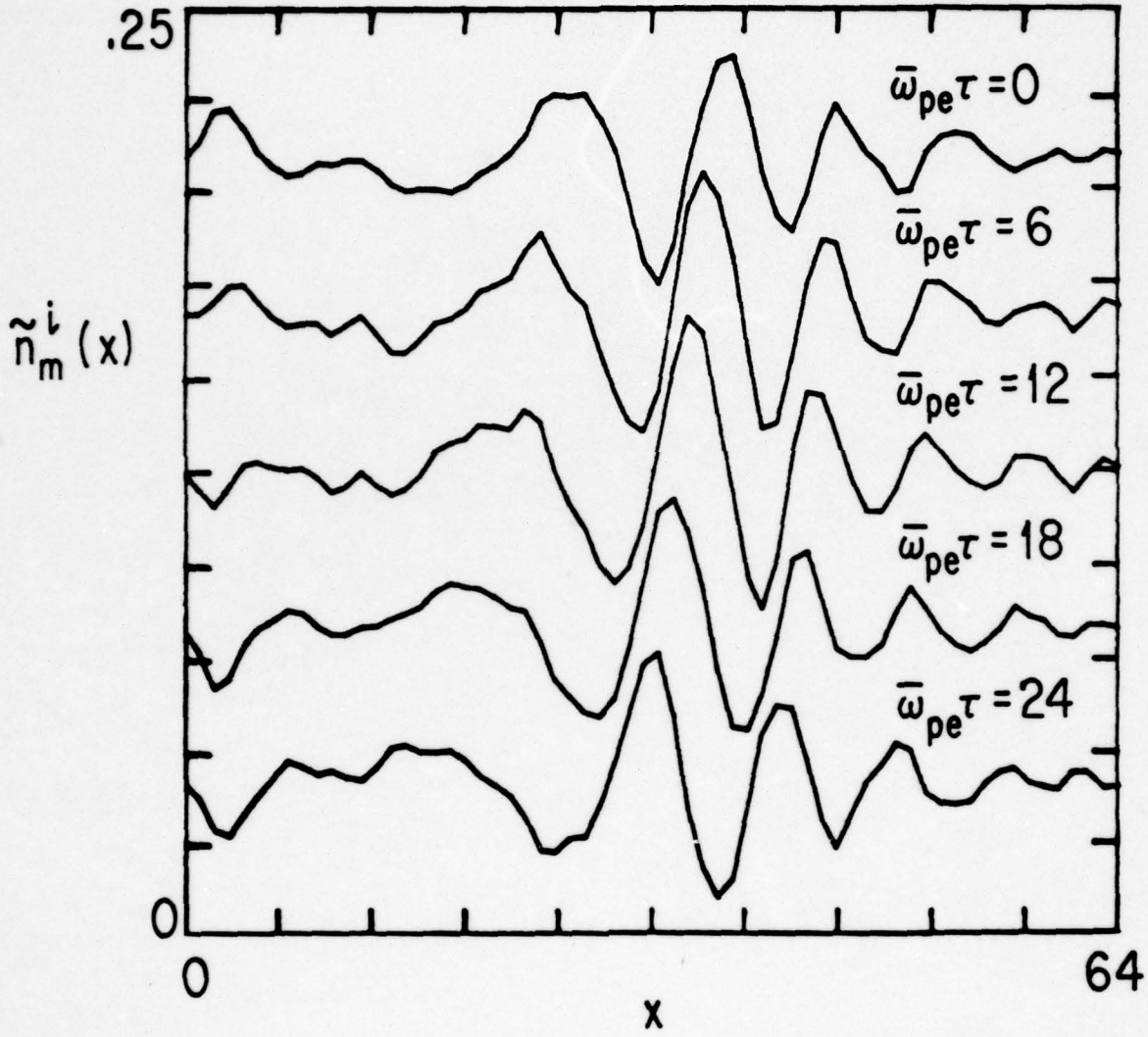
.25
0
0
64
x
$\tilde{n}_m^i(x)$
$\bar{\omega}_{pe}\tau = 0$
$\bar{\omega}_{pe}\tau = 6$
$\bar{\omega}_{pe}\tau = 12$
$\bar{\omega}_{pe}\tau = 18$
$\bar{\omega}_{pe}\tau = 24$

FIGURE 12

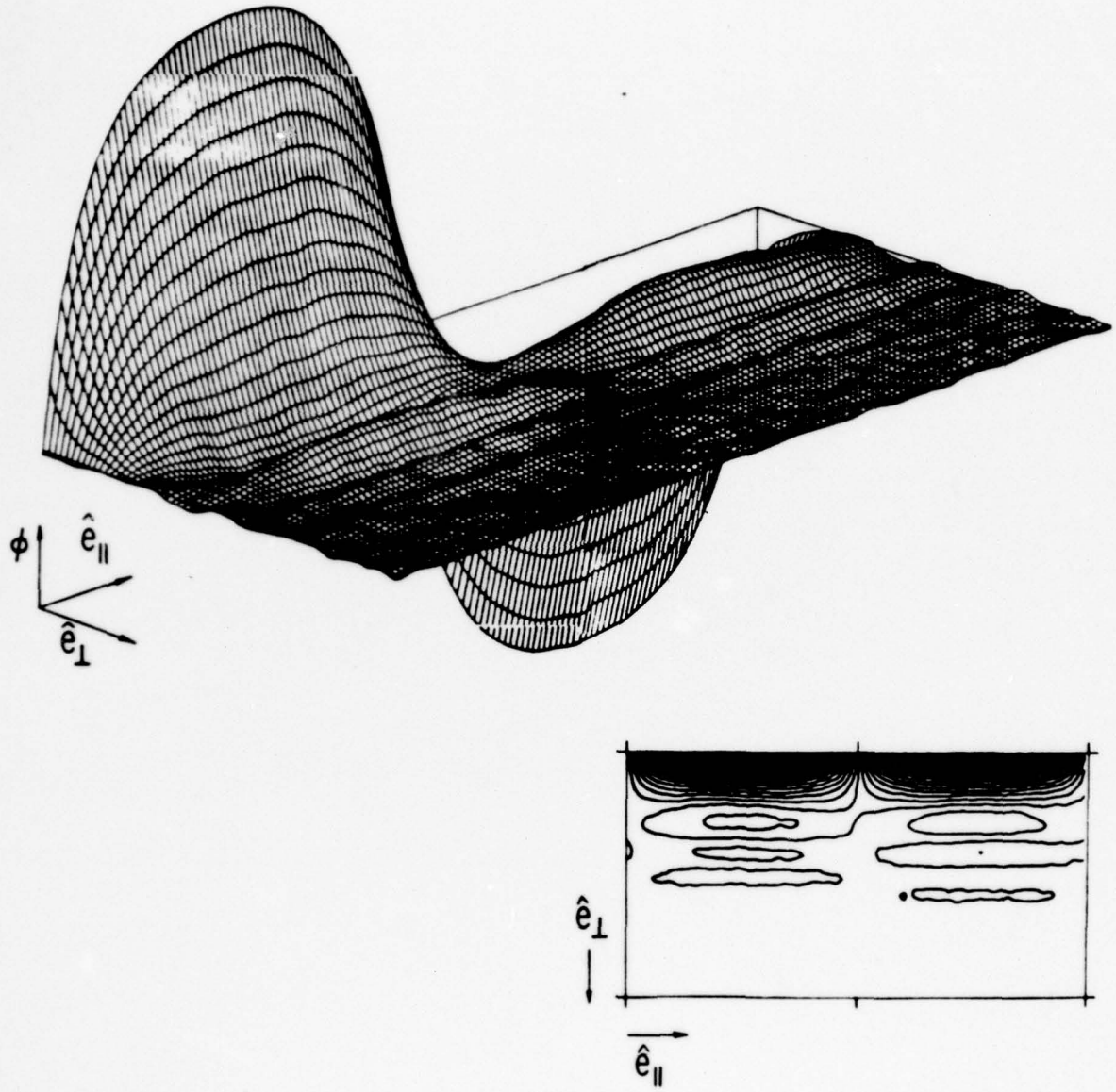

FIGURE 13

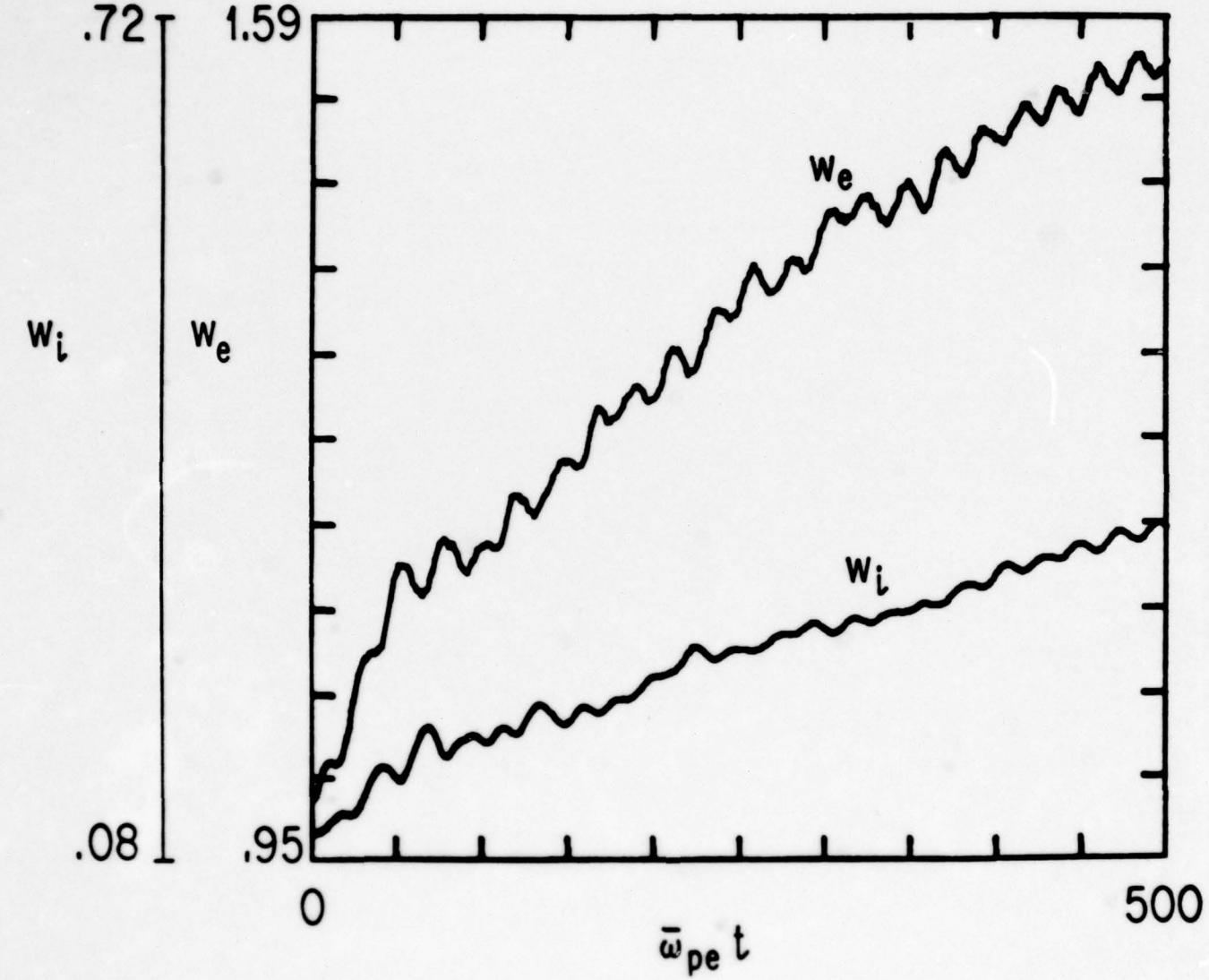

FIGURE 14

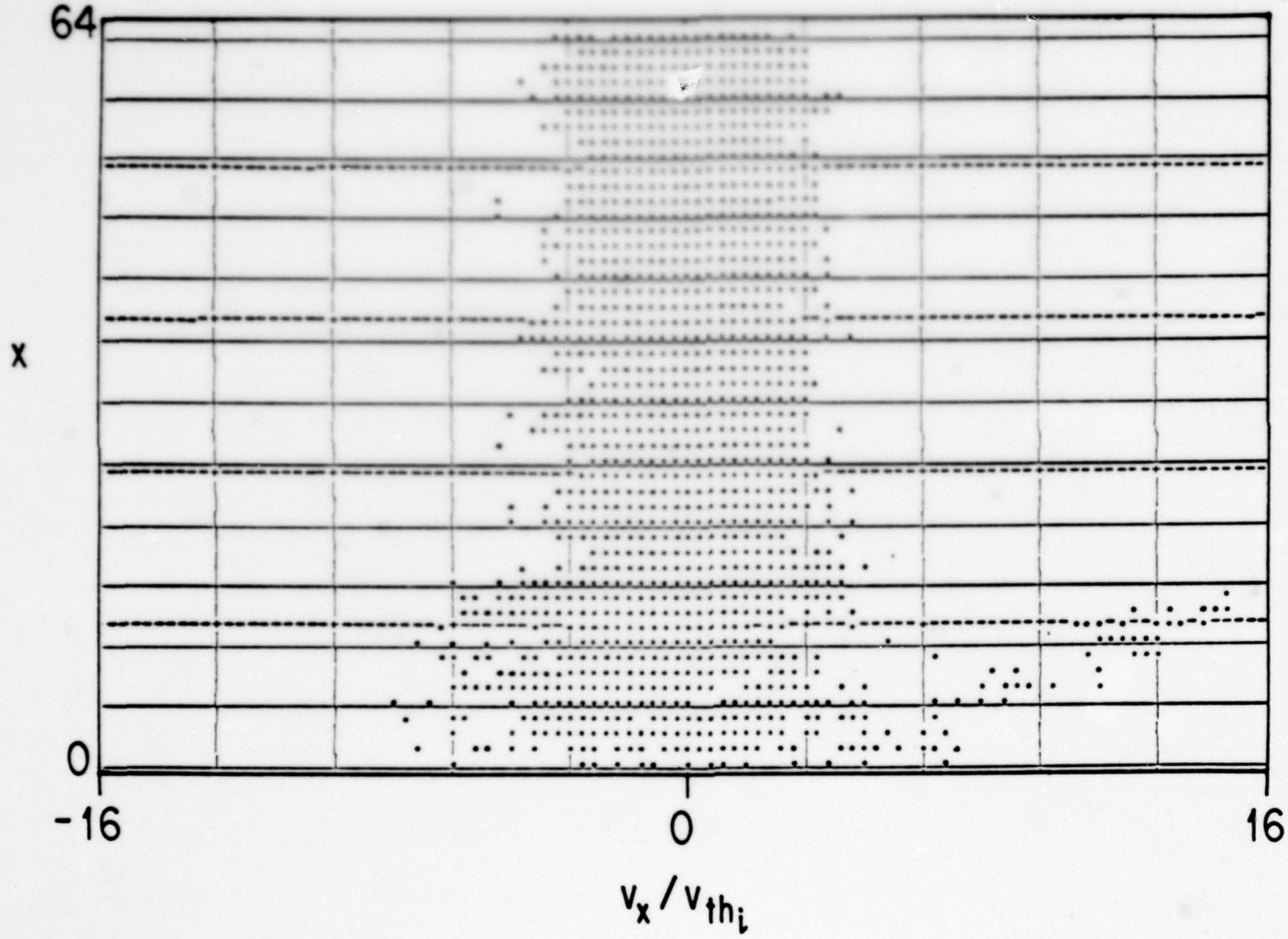

FIGURE 15

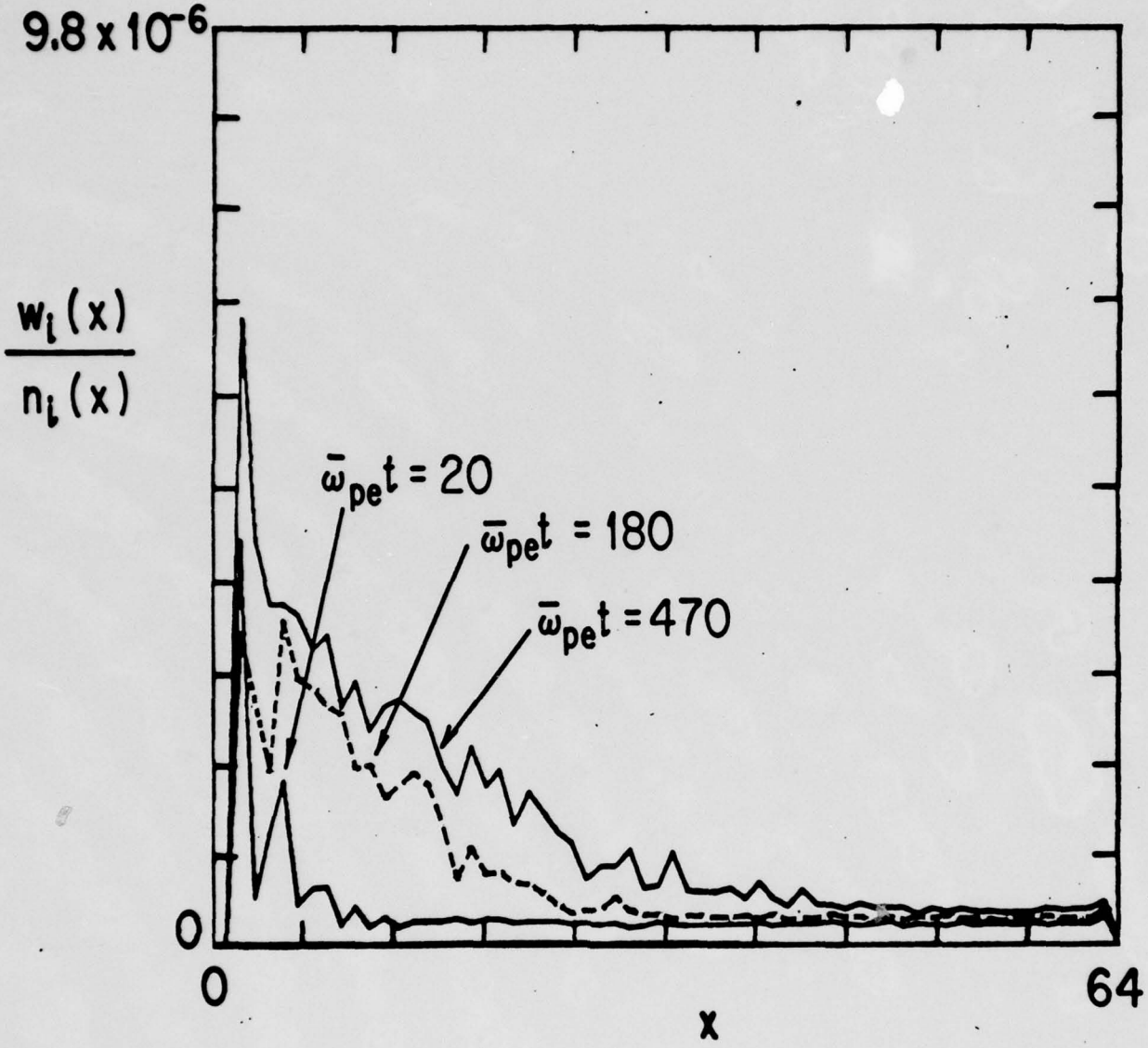

FIGURE 16

PPG-382 "Stimulated Brillouin Sidescatter and Backscatter of CO_2 Laser Radiation From a Laser-Altered Arc Plasma", Mark J. Herbst, dissertation, January (1979).

PPG-383 "Small-Scale Magnetic Fluctuations inside the Macrotor Tokamak", S. J. Zweben, C. R. Menyuk, and R. J. Taylor. Submitted to Phys. Rev. Lett., January (1979).

PPG-384 "A High Efficiency Free Electron Laser", A. T. Lin and J. M. Dawson. Submitted to Phys. Rev. Lett., January (1979).

PPG-385 "A Parametric Study of Electron Multiharmonic Instabilities in the Magnetosphere", M. Ashour-Abdalla, C. F. Kennel and W. Livesey. Submitted to J. of Geophys. Rev., January (1979).

PPG-386 "Global Formalism for Ballooning-Type Modes in Tokamaks", Y. C. Lee and J. M. VanDam, submitted to Phys. Rev. Lett., October (1978).

PPG-387 "On the Origin of Plasmaspheric Hiss: the Importance of Wave Propagation and the Plasma-Pause", R. M. Thorne, S. R. Church, and D. J. Gorney, submitted to Geophys. Res., January (1979).

PPG-388 "The New Alchemy Again -- Again", F. Chen, accepted by The Sciences, January (1979).

PPG-389 "Stability of Drift-Wave Eigenmodes with Arbitrary Radial Wavelengths", Y. C. Lee, Liu Chen and W. M. Nevins, submitted to Phys. Rev. Lett., February (1979).

PPG-390 "Alternate Concepts in Magnetic Fusion", Frank Chen, to be published in Phys. Today, February (1979).

PPG-391 "Enhanced Interaction between Electrons and Large Amplitude Plasma Waves by a DC Electric Field", J. N. Leboeuf and T. Tajima, accepted by Phys. Fluids, February, (1979).

PPG-392 "Coalescence of Magnetic Islands", P. L. Pritchett and C. C. Wu, submitted to Physics of Fluids, February (1979).

PPG-393 "Formation of Double Layers", P. Leung, A. Y. Wong and B. H. Quon. Submitted to Phys. Fluids, February (1979).

PPG-394 "Experiments on Magnetic Field Line Reconnection", R. L. Stenzel and W. Gekelman, submitted to Phys. Rev. Lett., February (1979).

PPG-395 "Magnetospheric Multiharmonic Instabilities", Maha Ashour-Abdalla, C. F. Kennel, and D. D. Sentman, to be published in the Proc. of the Symposium on Wave Instabilities in Space Plasmas, February (1979).

PPG-396 "Comment on the Ballooning Criterion for Multipoles", E. A. Adler and Y. C. Lee, to be submitted to Phys. Fluids, February (1979).

PPG-397 "Laser Electron Accelerator", T. Tajima and J. M. Dawson, submitted to Phys. Rev. Lett., March (1979).

PPG-398 "Pulsar Magnetospheres", C. F. Kennel, F. S. Fujimura, and R. Pellat, to be published in the Proceedings of NASA/JPL workshop on Planetary and Astrophysical Magnetospheres, a special edition of Space Science Reviews, March (1979).

PPG-399 "Nuclear Power as an Ultimate Power Source", F. Chen, March (1979).

PPG-400 "Experimental Observations of Highly Nonlinear States in Plasmas", by A. Y. Wong, April (1979).

PPG-401 "The Onset of Stochasticity in a Superadiabatic Mirror", by C. R. Menyuk and Y. C. Lee. To be submitted to Phys. Rev. Lett. and Phys. Fluids, April (1979).

PPG-402 "Linear Stability of High-m Drift-Tearing Modes", D. A. D'Ippolito, Y. C. Lee, and J. F. Drake, submitted to Phys. Fluids, March (1979).

PPG-403 "Aspects of Pulsar Evolution", F. S. Fujimura and C. F. Kennel, submitted to Astrophysical J., March (1979).

PPG-404 "A Magnetohydrodynamic Particle Code with Force Free Electrons for Fluid Simulations", T. Tajima, J. N. Leboeuf, and J. M. Dawson, submitted to J. of Computational Physics, April (1979).

PPG-405 "The Kelvin-Helmholtz Instability in Supersonic and Superalfvenic Fluids", by T. Tajima and J. N. Leboeuf, submitted to Phys. Fluids, April (1979).

PPG-406 "RF - Heating of Toroidal Plasmas", E. Canobbio, appears in Topics in Applied Physics (Springer-Verlag): Controlled Thermonuclear Fusion - Magnetic Confinement, April (1979).